Defensa de la tesis doctoral:

Defects and the vortex liquid state in superconducting textured $YBa_2Cu_3O_{7-d}$

Programa de Doctorat en Ciència de Materials
Departament de Física de la Universitat Autònoma de Barcelona

Per:
Jordi Figueras i Puig
Departament de Materials Magnètics i Superconductors
ICMAB-CSIC

Directors:Prof. Xavier Obradors
Dra. Teresa Puig
Tutor: Prof. Juan S.Muñoz Domínguez

Bellaterra, 15 de Juliol del 2003

Contents

1 Introduction **1**

1.1 Historical Remarks 1
1.2 Vortices in HTSC 6
1.2.1 Anisotropy 7
1.2.2 Influence of Microstructure 9
1.2.3 Thermal Energy 11
1.2.4 Phase Diagram and Vortex Dynamics 12
1.3 Phase diagram in $YBa_2Cu_3O_{7-\delta}$ single crystals. 19
1.4 Melt Textured Grown $YBa_2Cu_3O_{7-\delta}$ 22
1.4.1 Microstructural properties 22
1.4.2 Superconducting properties of MTG-$YBa_2Cu_3O_{7-\delta}$ 24

2 Experimental **27**

2.1 Growth 27
2.2 Post-processes and modifications on the preparation 29
2.3 Microstructural Characterization 31
2.3.1 Y_2BaCuO_5 particles 31
2.3.2 Twin Boundary density 33
2.3.3 Summary of the Microstructural Characteristics 36
2.4 Superconducting Properties 37
2.4.1 Inductive Measurements 37
2.4.2 Resistive Measurements 37

3 Magnetoresistive Measurements. **45**

3.1 Introduction 45
3.2 Single crystal $YBa_2Cu_3O_{7-\delta}$: a reference 46
3.2.1 Solid-Liquid Transition 46
3.2.2 Vortex dynamics 53
3.3 MTG-$YBa_2Cu_3O_{7-\delta}$ 58
3.3.1 Phase Diagram 58
3.3.2 Vortex dynamics 64
3.4 Related compounds 66

3.4.1 MTG-$YBa_2(Cu_{1-x}Mg_x)_3O_{7-\delta}$ . . . 66
3.4.2 MTG-$NdBa_2Cu_3O_{7-\delta}$ . . . 73
3.5 Conclusions . . . 78

4 Influence of Y_2BaCuO_5 particles **79**
4.1 Introduction . . . 79
4.2 Phase diagram . . . 81
4.3 Vortex Dynamics . . . 86
4.4 Conclusions . . . 92

5 In-plane dislocations **95**
5.1 Introduction . . . 95
5.2 Out of plane measurements . . . 100
5.3 In-plane measurements . . . 103
5.3.1 In-plane measurements for an as-grown sample . . . 103
5.3.2 In-plane results for an HOP sample . . . 107
5.4 Conclusions . . . 111

6 Vortex Breaking defects **113**
6.1 Introduction . . . 113
6.2 Influence of microcracks . . . 116
6.2.1 Magnetic phase diagram . . . 116
6.2.2 Vortex Dynamics . . . 119
6.3 Influence of stacking faults . . . 123
6.4 Comparison between both planar defects . . . 125
6.5 Conclusions . . . 126

7 Twin Boundaries **129**
7.1 Introduction . . . 129
7.2 Phase diagram . . . 131
7.2.1 Irreversibility line . . . 131
7.2.2 Region of influence of twin boundaries in the vortex liquid state . . . 135
7.3 Vortex dynamics . . . 139
7.4 Conclusions . . . 143

8 Vortex liquid phase diagram **145**
8.1 Introduction . . . 145
8.2 Scaling of the measurements . . . 146
8.3 Vortex correlation . . . 151
8.3.1 Flux Transformer measurements . . . 151
8.3.2 Discussion . . . 158
8.4 Conclusions . . . 163

9 Conclusions **165**

Acknowledgements

To Prof. Xavier Obradors and Dr. Teresa Puig, supervisors of this thesis. Thanks for the opportunity to work in an amazing field of research.Thanks for the confidence that they have demonstrated, for their collaboration and help. For introducing me in a new world and offer the opportunity to meet great people around the world.

To those, who, since the beginning of this work, have worked in the Department of Magnetic and Superconducting Materials. Thanks for the opportunity to learn a part of their multidisciplinary knowledge.

To Prof. G.W.Crabtree and Dr.K.Kwok, for allowing to stay three months in the Argonne National Laboratory. The chance to work in the Materials Science Division will not be forgotten. I also thank Dr.B.Olsson for his experimental support while preparing and performing the measurements.

To the fellows of our Department Anna Esther Carrillo, Ernest Mendoza and Jerome Plain, for preparing and transferring the high quality samples investigated in this work. In particular, I would like to thank J.Plain and E.Mendoza for many interesting discussions about the superconducting properties of MTG materials.

To the Generalist de Catalunya, for financial support.

To the colleges and friends of the Department, thanks for their energy, promoting a good climate of work. Without their support, this work would not be finished.

To those who shared with me countless lunches in the *cafeteria*, creating an small oasis during the day.

I finalment, a la familia, per tot el que m'han donat.

Whatever stopped you from dreaming,
whatever tried to stop you from living,
flip it.

Alicia Keys

Preface

The discovery of High Temperature Superconductors gave birth to a complex phenomenology in the field of vortex physics of Type II superconductors. High Temperature superconductors due to the large penetration depth, short coherence length, large thermal energies and the strong anisotropy lead to a completely new phenomenology which requires a careful investigation.

In the mixed state of High Temperature Superconductors, several energies of similar magnitude are competing: vortex-vortex interaction, 3-D coupling energy, vortex pinning energy and the thermal energy. This competition gives place to a magnetic phase diagram with different phases depending on the particular value of these interactions.

$YBa_2Cu_3O_{7-\delta}$ has been one of the most investigated HTSC superconductors due to their potential applications. The influence of microstructure has been widely studied in $YBa_2Cu_3O_{7-\delta}$ single crystals where artificial and controlled pinning centers have been successfully generated by irradiation. Their effects have been studied in terms of the dimensionality of the pinning centers that have been introduced in the sample.

$YBa_2Cu_3O_{7-\delta}$ single crystals, however, and due to their small size are not suitable for applications. To obtain large sized samples, Melt Texturing processing technologies have been developed. Melt Textured Grown (MTG) $YBa_2Cu_3O_{7-\delta}$ samples possess a much higher density and diversity of defects. The properties of vortices in MTG-$YBa_2Cu_3O_{7-\delta}$ samples (with a wide diversity of microstructural defects capable of modifying vortex behavior) is certainly worth of study. The goal of this thesis is to investigate the influence of the microstructure on the superconducting properties of MTG-$YBa_2Cu_3O_{7-\delta}$, focussing in the vortex liquid state.

In this sense, in *chapter 1* we will describe the main properties concerning vortices of HTSC. In particular, the results obtained previously in $YBa_2Cu_3O_{7-\delta}$ will be reported. The main defects present in Melt Textured Grown $YBa_2Cu_3O_{7-\delta}$ samples are also revealed.

In *chapter 2* the experimental tools that have been used to characterize the samples and study their superconducting properties are explained.

In *chapter 3* the capability of magnetoresistance measurements in order to obtain the magnetic phase diagram and the properties of vortex motion will be shown. In particular, a twinned $YBa_2Cu_3O_{7-\delta}$ single crystal and a Melt Textured $YBa_2Cu_3O_{7-\delta}$ sample are studied. The similarities and differences on the superconducting properties will be analyzed. Systems such as $YBa_2(Cu_{1-x}Mg_x)_3O_{7-\delta}$ and $NdBa_2Cu_3O_{7-\delta}$ with intrinsic properties different than those of $YBa_2Cu_3O_{7-\delta}$ will also be investigated and compared.

In *chapters 4*-7, the influence of the main microstructural defects present in Melt Textured Grown samples on the magnetic phase diagram and vortex motion in the liquid state will be widely investigated. In particular *chapter 4* investigates the influence of the main microstructural defect present in MTG-$YBa_2Cu_3O_{7-\delta}$ samples: $Y_2BaCuO_5/YBa_2Cu_3O_{7-\delta}$ interfaces. In *chapter 5* the influence of in-plane dislocations, either as linear-like or point-like pinning centers is considered. In *chapter 6* the influence of microcracks and stacking faults as detrimental microstructural defects is investigated. Finally, in *chapter 7* the influence of twin boundaries as linear-like pinning centers is analyzed.

In *chapter 8*, the general features observed in the previous chapters will be studied and compared. The similarities found will be further explored in order to build our picture of the vortex liquid phase diagram in $YBa_2Cu_3O_{7-\delta}$.

Finally, in *chapter 9*, the conclusions of the present work will be summarized.

Chapter 1

Introduction

1.1 Historical Remarks

Two main properties characterize the existence of superconductivity. The first one is the lack of any electric resistance for the material at temperatures below a certain critical temperature (T_c) [1]. In normal conducting materials, the appearance of resistivity is related to the existence of scattering between the carriers (either being electrons or holes) against impurities or phonons. In superconductors, however, the carriers are coupled forming Cooper pairs which, behaving as bosons, fall into the ground state forming a Bose condensate. These Cooper pairs will not be scattered and therefore, zero resistance is obtained. The condensate that results from this coupling is represented by a wave function (Ψ) that changes in a distance given by the coherence length, $\xi(T)$.

The other feature that characterizes the superconducting state is the complete expulsion of the applied magnetic field from the sample at temperatures below the critical temperature. The expulsion is produced by Cooper pairs circulating at the surface of the sample, that are able to screen the external magnetic field. These currents penetrate into the sample a depth characterized by the penetration length, $\lambda(T)$, leading to the exponential decay of the magnetic field shown in figure 1.1. The complete expulsion of the magnetic field from the sample is known as the Meissner effect.

By considering these two quantities (ξ and λ), the different superconducting materials can be classified as follow:

1. $\kappa = \frac{\lambda(T=0K)}{\xi(T=0K)} \leq \frac{1}{\sqrt{2}}$:Type I superconductors
   In these materials and for magnetic fields below a certain critical field, H_c(T) (see figure 1.2 left), the appearance of Meissner currents impedes the penetration of the magnetic field into the sample. Above this magnetic field, the binding energy of the pairs becomes zero, and therefore, Cooper pairs are unstable bringing the sample into the normal state.

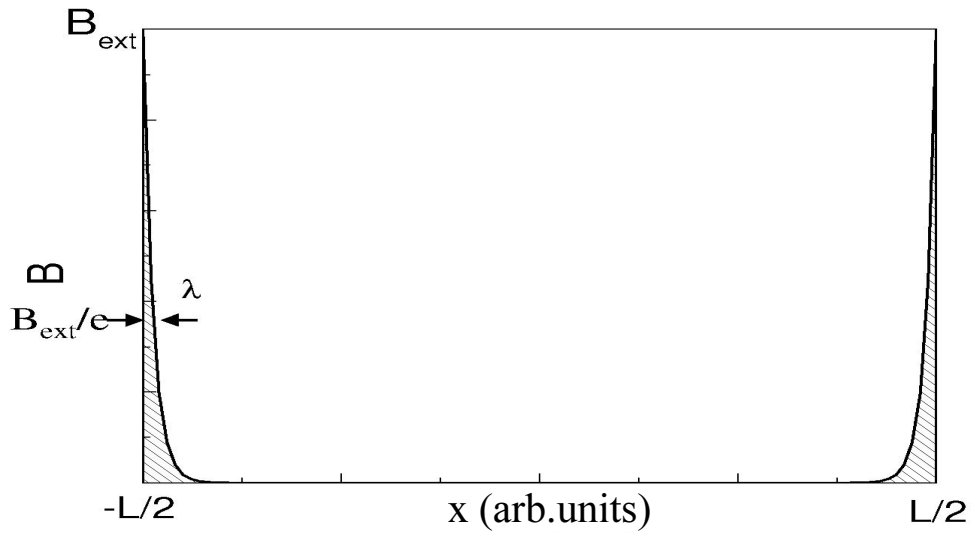

Figure 1.1: Profile of the magnetic field in the Meissner state of a superconducting sample. The decrease of the magnetic field inside the superconductor is given by the penetration depth, λ.

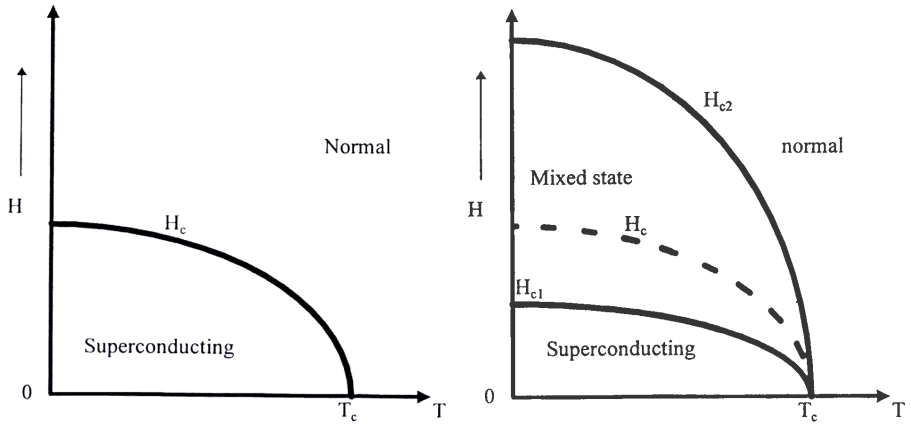

Figure 1.2: Magnetic phase diagram for Type I (left) and Type II (right) superconductors.

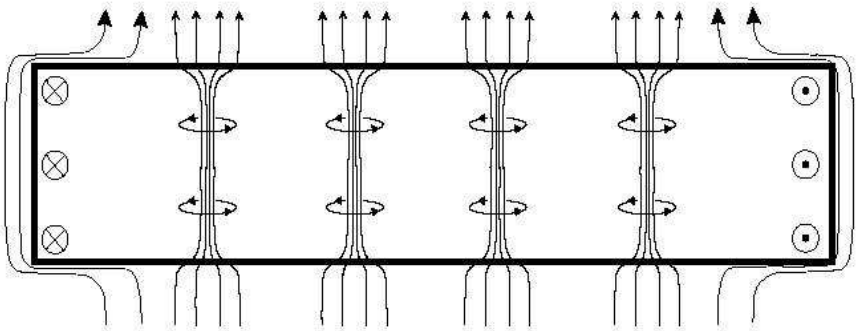

Figure 1.3: Schematic representation of the magnetic flux inside a type II superconductor in the mixed state. Flux lines penetrate into the sample in a quantized form, as vortices.

2. $\kappa = \frac{\lambda(T=0K)}{\xi(T=0K)} \geq \frac{1}{\sqrt{2}}$:Type II superconductors
   Type II superconductors are characterized by two different critical fields, H_{c_1} and H_{c_2} (see figure 1.2 right). For magnetic fields below the low critical field, H_{c_1}(T), and similarly to that observed in type I superconductors, Meissner currents are flowing at the surface disabling the magnetic field to penetrate into the sample. As the magnetic field is increased above H_{c_1} (T), but still below the upper critical field, H_{c_2} (T), there exists penetration of the magnetic field inside the superconducting sample (mixed state). This penetration is produced in the form of quantized vortices [2], i.e., as lines of magnetic flux crossing the sample, each one containing a quantum of flux $\Phi_0 = 2.07 \cdot 10^{-7} G \cdot cm^2$. An schematic representation of the penetration of these flux lines (vortex) into the sample, is shown in figure 1.3. These vortices are formed by a core of unbinded charge carriers surrounded by superconducting currents, as shown in figure 1.4. Further increasing the magnetic field, the number of vortex inside the sample increases and at the upper critical field H_{c_2}, the cores of the neighbouring vortex overlap and thus, the sample goes to the normal state.

A second division of superconducting materials is done when considering its critical temperature, by distinguishing superconductors of low critical temperature (LTSC) from high temperature superconductors. All high temperature superconductors (HTSC) are type II superconductors.

In low T_c superconductors, charge carriers are coupled via electron-phonon and are fully described by the theory developed by Bardeen,Cooper and Schiffer [3]. In high temperature superconductors, however, the interaction between charge carriers and phonons cannot (on its own) explain the large energies required to break the Cooper pairs. The existence of another mechanism promoting the formation of Cooper pairs in high temperature superconductors is then required. The search for the origin of this interaction in HTSC has been one of the main items since the discovery of the first high temperature superconductor: $(La,Ba)_2Cu_4$

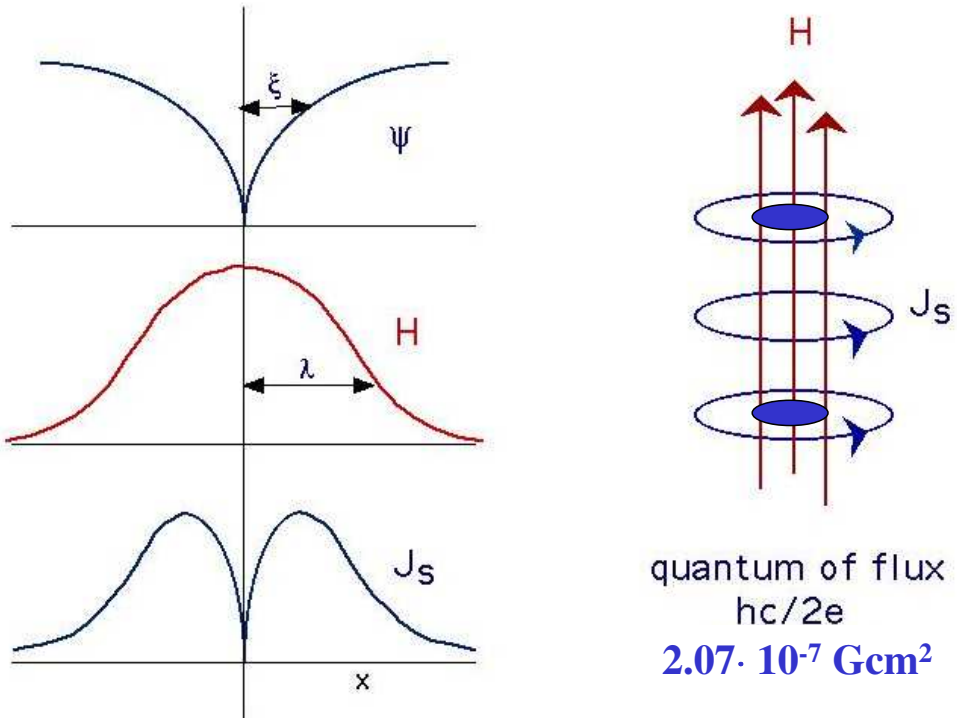

Figure 1.4: Left: Scheme of the profile of the wave function (Ψ), the magnetic field (H) and the distribution of supercurrents (J_s) inside a vortex. At the right: structure of the vortex formed by a normal core and surrounding supercurrents.

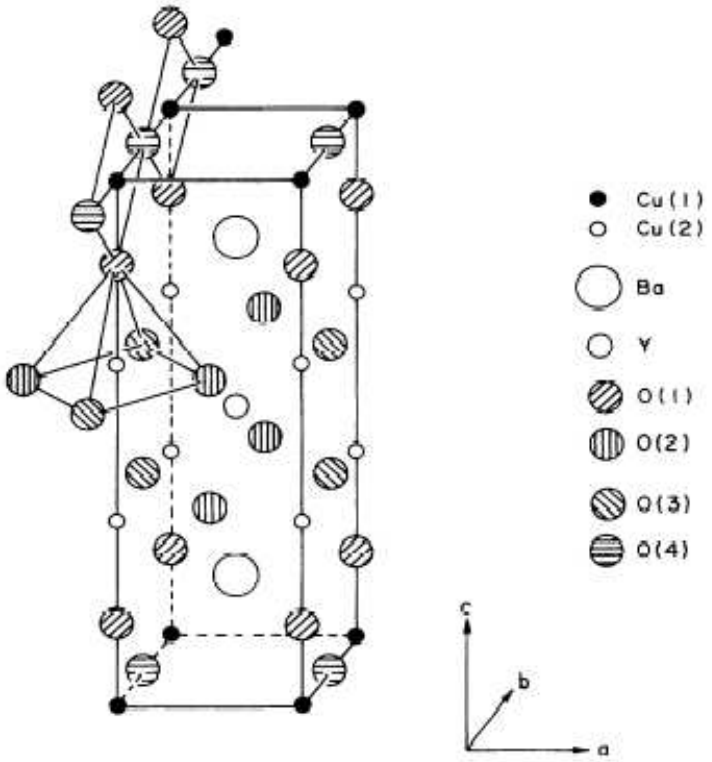

Figure 1.5: Crystallographic structure of $YBa_2Cu_3O_{7-\delta}$ [7].

(T_c =37K), the year 1986 [4]. Different possible mechanisms originating high T_c superconductivity are presently under debate [5, 6].

HTSC superconductors, in contrast to LTSC, have a layered structure where their principal characteristic is the existence of CuO_2 planes (see figure 1.5), that determines the superconducting properties of the cuprates. Moreover, the discovery of $(La,Ba)_2CuO_4$ started a race in order to find new materials with similar structure and higher T_c. A few months later, $YBa_2Cu_3O_{7-\delta}$ was discovered with $T_c \approx 92K$. This new superconductor, being the first material with a critical temperature above the temperature of liquid nitrogen, drastically reduced the cost of the cryogenics involved. Although the critical temperature of $YBa_2Cu_3O_{7-\delta}$ has been surpassed by far in other cuprates (it reaches T_c =138K in $Hg_{0.8}Tl_{0.2}Ba_2Ca_2Cu_3O_{8+\delta}$), the higher anisotropy of these other systems is a severe drawback for their application. Since then, several other families of superconductors have been discovered, with new characteristics and properties (in figure 1.6 it is shown the evolution in T_c in some families of superconductors). In January 2001, a compound with a fairly simple structure, MgB_2, was announced to be superconducting with $T_c \approx 39K$[8]. The appearance of such a high T_c non-cuprate

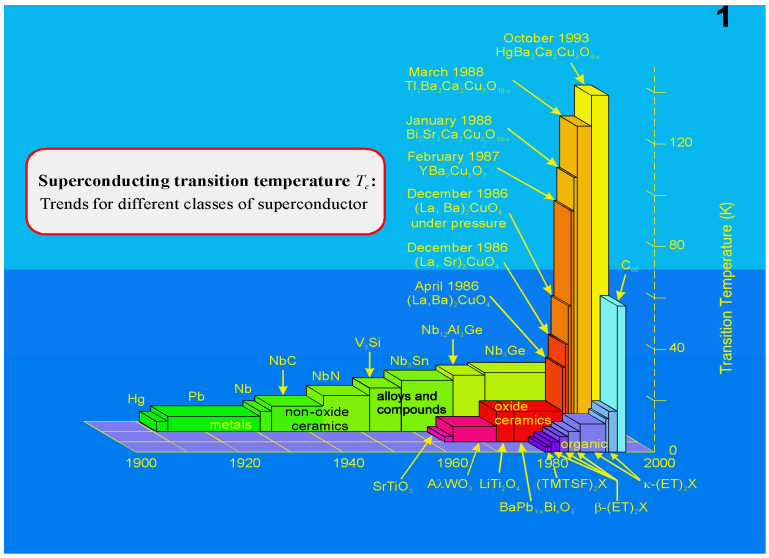

Figure 1.6: Critical Temperature for several systems as a function of the year of discovery.

superconductor provided another system capable to enable the study of the mechanisms responsible of superconductivity. The search for materials with similar structure and higher T_c has not been successful and MgB_2 has become a special material with unique characteristics. Another class of superconductors widely investigated are organic superconductors, where *buckyballs* (C60) have been the most studied materials [9].

1.2 Vortices in HTSC

Vortex motion is strongly enhanced in HTSC due to the large thermal energies present. Thus, vortex dynamics in high temperature superconductors has to be understood and controlled in order to enable the possible application of these materials since the motion of the cores (formed by non-superconducting carriers) leads to dissipation. The high temperatures involved and the large anisotropy of HTSC strongly increases vortex motion. Fortunately, the interaction between vortices and microstructural defects with the superconducting properties strongly suppressed may act as vortex pinning centers and stabilizes vortices against motion, and therefore improve superconducting properties in these systems. In order to obtain a strong influence of microstructure, however, it is required that the size of the defects is similar to that of the coherence length ($\xi_{ab} \approx 10 - 20$Å for cuprates). Therefore, a control of the microstructure in the nanometric scale is required and thus becomes difficult to improve the superconducting properties.

Moreover, the competition between different interactions of similar energies, generates new physics, having some important similarities with other systems (such as bosons or poly-

mers). Therefore, vortex physics in high temperature superconductors has become a very rich research field with a broad spectrum of new phenomena and ideas, particularly concerning vortex dynamics[10]. These interactions and their influence on vortex behavior are discussed in the following.

1.2.1 Anisotropy

As already mentioned, the laminar structure of cuprates (see figure 1.5) leads to a highly anisotropic behavior, both in the normal state, with a resistivity much higher along the c-axis than that of the ab-plane ($\frac{\rho_c}{\rho_{ab}} \sim 50$ in $YBa_2Cu_3O_{7-\delta}$), and in the superconducting state, where the presence of a magnetic field along the c-axis is much more destructive than a magnetic field parallel to the ab-plane (for instance, H_{c_2} is strongly anisotropic).

The anisotropic behavior may be described with two different effective masses of the Cooper pairs, depending on the direction (m^*_{ab} and m^*_c) of the magnetic field, and therefore, an anisotropy factor $\gamma^{-1} = \sqrt{\frac{m^*_c}{m^*_{ab}}}$ may be defined. The anisotropy factor can be as high as $\gamma^{-1} \sim 100$ in $Bi_2Sr_2Ca_2Cu_3O_{10}$, while for $YBa_2Cu_3O_{7-\delta}$ values $\gamma^{-1} \sim 5-8$ have been reported. This anisotropy factor has been shown to be determined by the distance between CuO_2 planes, as shown in figure 1.7, in agreement with a charge transfer by tunnel effect along the c-axis. The anisotropy of $YBa_2Cu_3O_{7-\delta}$, however, is better explained when considering the distance between the CuO_2 planes and the CuO chains, indicating that the metalicity of the chains play a crucial role in the low anisotropy of this compound.

The anisotropy of these layered superconductors leads to a different geometry of the vortex along the ab-plane or the c-axis (as shown in figure 1.8), being elongated along the ab-plane. Furthermore, these distances, and in particular ξ_c (the coherence length along the c-axis), determines whether the vortex has an anisotropic character, but still a 3-D behavior or simply it has a 2-D character, with a very small correlation (if any) along the c-axis. The condition for a 2-D system is:

$$s > \frac{\xi_{ab}}{\gamma^{-1}}, \tag{1.1}$$

since then, the discrete nature of the system will modify vortex structure (as seen in figure 1.8), and a reduced coupling along the c-axis will be manifested.

In materials not extremely anisotropic, such as $YBa_2Cu_3O_{7-\delta}$, the temperature where the condition 1.1 is fulfilled are below $T = 0.75T_c$, therefore vortices are still 3-D entities in the temperature range investigated, and the behavior can be scaled [12] using an effective magnetic field given by:

$$H_{eff} = \varepsilon_\theta H, \tag{1.2}$$

where $\varepsilon_\theta = \sqrt{\gamma^2 \cdot \sin^2(\theta) + \cos^2(\theta)}$, and θ is the angle comprised between the crystallographic c-axis and the magnetic field, as shown in figure 1.9. Therefore, we obtain for H$\|$c

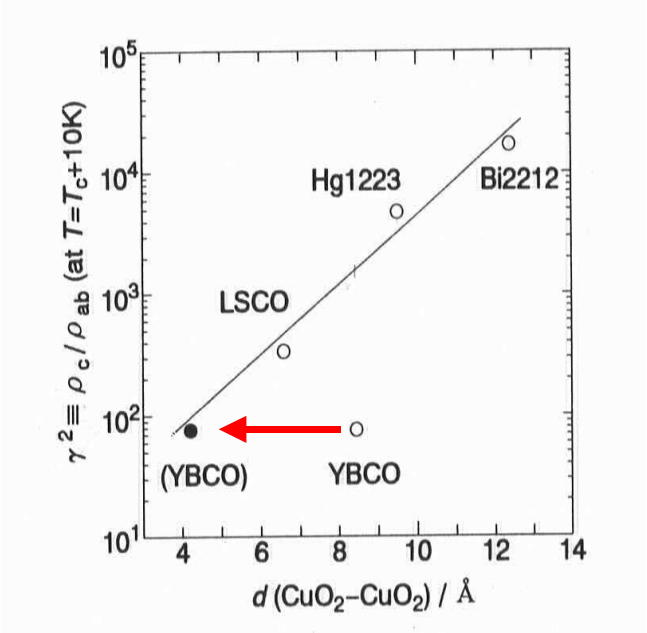

Figure 1.7: Dependence of the anisotropic parameter γ^{-1} with the distance between CuO_2 layers. As it becomes apparent in the figure, the anisotropy of $YBa_2Cu_3O_{7-\delta}$ instead is determined by the distance between CuO_2 planes and CuO chains [11].

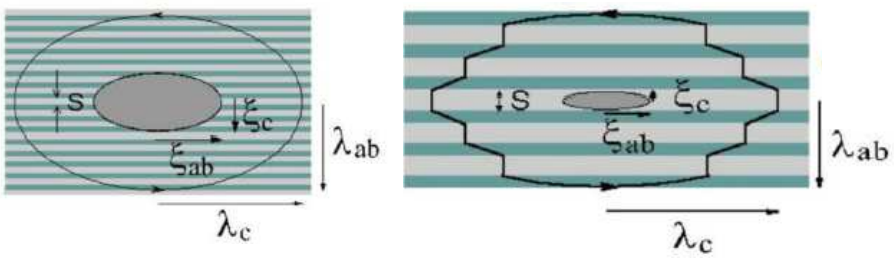

Figure 1.8: Structure of a 3-D (left) and a quasi 2-D (right) vortex lying parallel to the ab-plane.

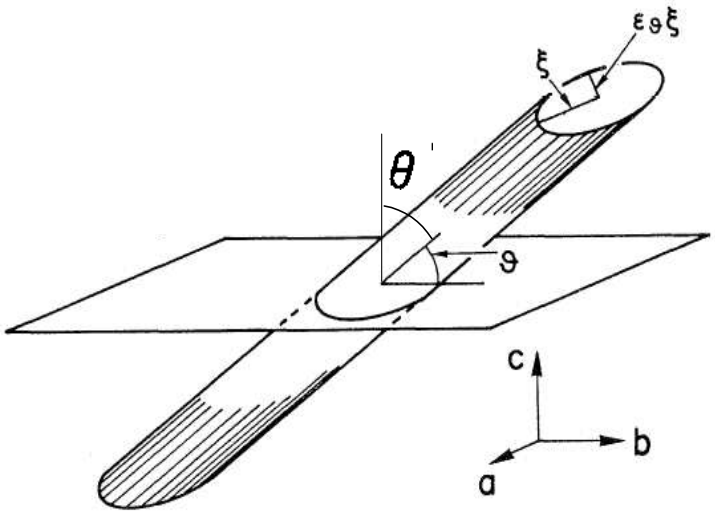

Figure 1.9: Scheme of a vortex aligned to a direction forming an angle θ with respect to the crystallographic c-axis [10].

($\theta = 0^o$) H_{eff}=H, while for H||ab ($\theta = 90^o$) we obtain $H_{eff} = \gamma \cdot H < H$. The validity of this scaling of the magnetic field has been thoroughly investigated in this thesis.

1.2.2 Influence of Microstructure

Surrounding the core of the vortex, there are the supercurrents which generate a magnetic field inside the core. Therefore, there exists a strong, repulsive magnetic interaction between vortices that tends to push them apart. This vortex-vortex repulsion promotes, in an homogeneous sample at low temperature, the formation of a regular [2], triangular lattice (Abrikosov lattice), both in low T_c and high T_c type II superconductors. An experimental observation of the Abrikosov lattice is shown in figure 1.10. In HTSC, however, the coherence length is much shorter ($\xi_{ab} \sim 15$Å in $YBa_2Cu_3O_{7-\delta}$) than in LTSC and coincides with the dimensions of the atomic defects that exist in the sample. The region around the microstructural defects have detrimental superconducting properties leading to a decrease of the formation energy of the vortex core, required to destroy the Cooper pairs. Therefore, the presence of microstructural defects modifies the underlaying background potential (as schematically represented in figure 1.11) to which the vortex is submitted and the long range order associated to the Abrikosov lattice may be destroyed. If the disorder is small, the long range order will be still preserved forming a Bragg-glass [14], but for a large enough disorder, the long range order will be lost and the vortices will be arranged forming a glass.

It has been argued that, depending on the shape and dimensions of the microstructural defect, defects may act as point-like or linear-like pinning centers:

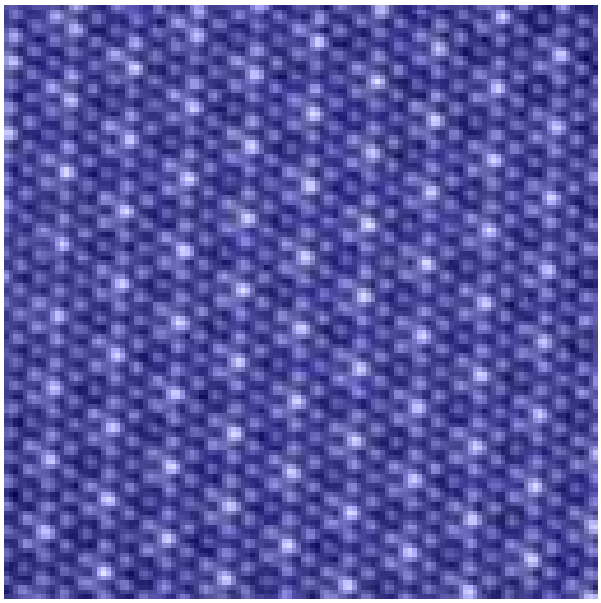

Figure 1.10: Abrikosov lattice as observed in $NbSe_2$ by Scanning Tunneling Microscopy by Davis et al.[13]

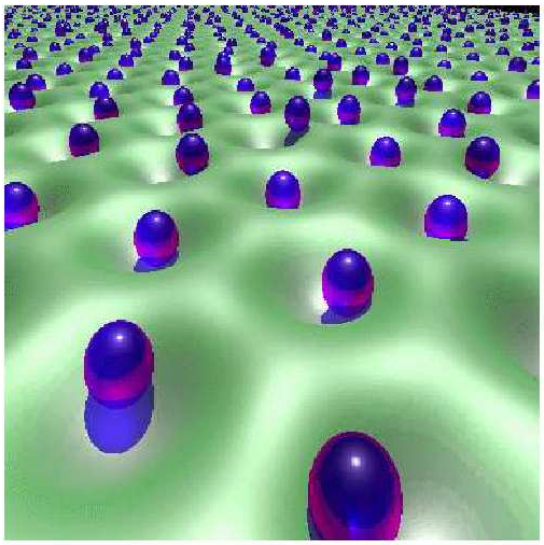

Figure 1.11: Schematic representation of the pinning potential related to the presence of microstructural defects and the vortex-vortex interaction, together with the position of different vortex[15].

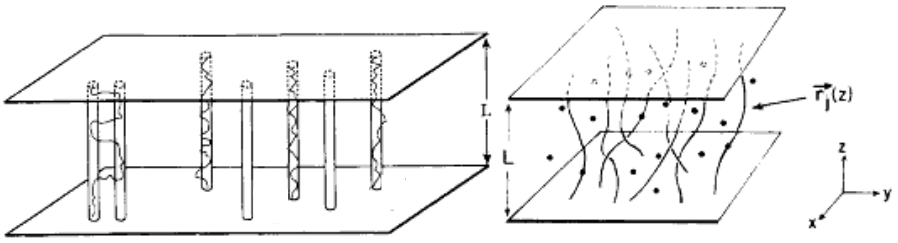

Figure 1.12: Influence of linear like (left) [17] and point like defects (right) [18] on vortex position.

Point-like pinning centers, when the defect has dimensions of the order of the coherence length. Consequently, the region where the defect is present will have suppressed superconducting properties and will act as a point-like pinning center (see figure 1.12). The disorder introduced can promote a vortex-glass [16].

Linear-like pinning centers, when one of the dimensions of the defect (parallel to the vortex) is larger than the coherence length while the other two are of the order of ξ_{ab}. The vortex will, therefore, be pinned over a large length (see figure 1.12), forming a Bose-glass[17].

However, microstructural defects may also have a detrimental influence on vortex motion. In this sense, grain boundaries, separating regions with different orientations of the crystallographic structure have been shown to strongly reduce the superconducting properties [19]. In particular it has been found that the maximum current that may flow across a tilt grain boundary (prior to dissipation) decreases exponentially with the misorientation angle between grains for angles larger than 5-10°. The presence of microcracks or stacking faults may also lead to a reduction of the superconducting properties. Their influence at high magnetic fields and high temperatures will be studied in this thesis (chapter 6).

1.2.3 Thermal Energy

As already mentioned (and as represented in figure 1.11), vortices present in the sample are submitted to two distinct forces: vortex-vortex and vortex-defect interaction. The strong thermal energies of HTSC, however, may enable vortices to easily overcome the pinning potential. The consequent vortex depinning leads to an effective motion of vortices even for a vanishingly small force.

In magnetoresistance measurements (for current perpendicular to the applied magnetic field), the small force promoting vortex motion is given by the presence of a small current. Considering an applied current (I) vortices will be submitted to a Lorentz force given by:

$$F_L = I \cdot \Phi_0 \cdot \sin(\alpha), \tag{1.3}$$

where α is the angle formed by the current and the magnetic field, and $\Phi_0 = 2.07 \cdot 10^{-7} G \cdot cm^2$ is the magnetic flux quantum. At low temperatures, a large current is required to promote vortex motion, but at high enough temperatures, a certain number of vortices will be thermally depinned. The number of depinned vortices is given by:

$$N_{dep} = N_0 e^{-\frac{U(T)}{kT}}, \tag{1.4}$$

with U(T) the vortex activation energy and N_0 the number of vortex present in the sample. The motion of these vortices generates a resistivity given by [20, 21]:

$$\rho = \rho_0 e^{-\frac{U(T)}{kT}}, \tag{1.5}$$

is then obtained. Therefore, from the temperature dependence of the resistivity, we may determine the vortex activation energy, i.e. the potential barrier that vortices have to overcome to start moving.

1.2.4 Phase Diagram and Vortex Dynamics

In addition to the existence of a high anisotropy and the presence of defects being capable to act as pinning centers, we have shown that the high thermal energies involved in these systems have a strong influence on the behavior of vortices in these samples. These facts strongly modify the characteristics that were found previously in low T_c superconductors, producing a qualitatively different magnetic phase diagram. Their mutual influences over vortices may be summarized as follow (and represented in figure 1.13):

Vortex-Vortex Energy: Promotes the existence of a ordered solid.

Coupling Energy: Promotes the decoupling of vortices along the c-axis.

Thermal Energy: Vortex depinning is enhanced and therefore a vortex liquid appears.

Vortex pinning Energy: Distorts the vortex lattice into a glass of vortices.

The coexistence of these energies, very similar in value, in any high temperature superconductor, produces a strong diversity of phases, as represented in figure 1.14. Furthermore, since their strength depend on the particular point of the magnetic phase diagram considered, it follows that different phases may appear, even in a single sample. Therefore, a very complex phase diagram is formed, which changes from sample to sample depending on its particular microstructure. For a fixed anisotropy (this parameter will not be essentially modified through the thesis), thermal energy, pinning energy and vortex-vortex interaction will compete. At low temperatures, the vortex pinning energy at which the vortex is submitted is dominant over the thermal energy and a solid vortex state is formed. However, at this low temperature solid vortex state, and depending on the competition between the vortex-vortex

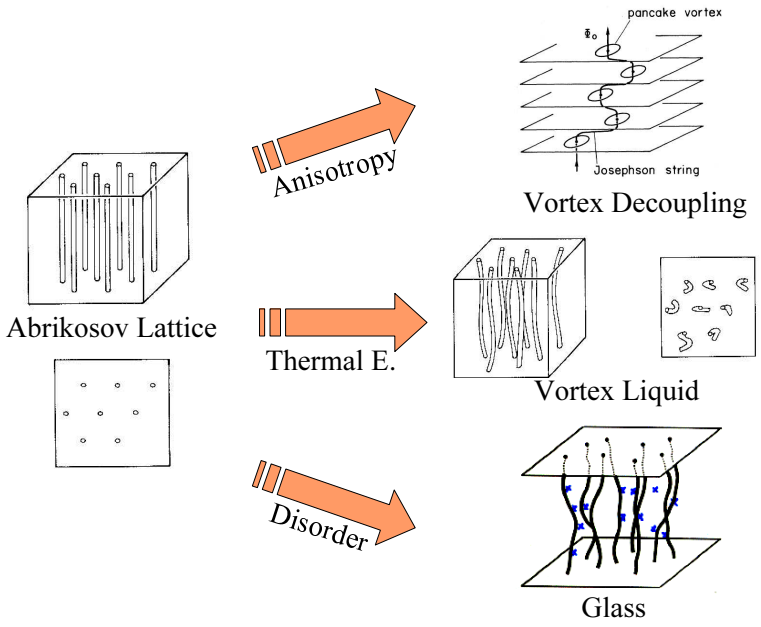

Figure 1.13: Influence of the anisotropy, the thermal energy and the microstructure over vortices (adapted from [10]).

interaction and disorder, two different options appear. At low disorders, long range order (either an Abrikosov lattice or a Bragg-glass) is still preserved, while at high enough disorder, a glass will be formed.

As increasing the temperature, a transition in the phase diagram appears, that can be a first order transition (melting) or a second order transition, depending on the density of defects present in the samples. This transition separates a solid vortex state from a liquid vortex state (see figure 1.14):

Solid Vortex State: The vortex thermal energy is lower than the energy barrier given by the vortex-vortex interaction and vortex-pinning interaction. A finite force is required in order to promote vortex motion.

Liquid Vortex State: The vortex thermal energy is large enough to overcome the background potential. Vortex easily move when applying external forces (even in the limit of a vanishingly small force). However, just above the solid-liquid transition, the pinning energy is still able to compete against the thermal energy and modify vortex motion. This situation will be the one considered in this thesis.

Two kinds of solid-liquid transition, however, may be clearly differentiated, depending on the nature of the low temperature phase: the vortex lattice (or Bragg glass), will transform into a liquid through a first order transition (vortex melting)[22–25]. As the disorder

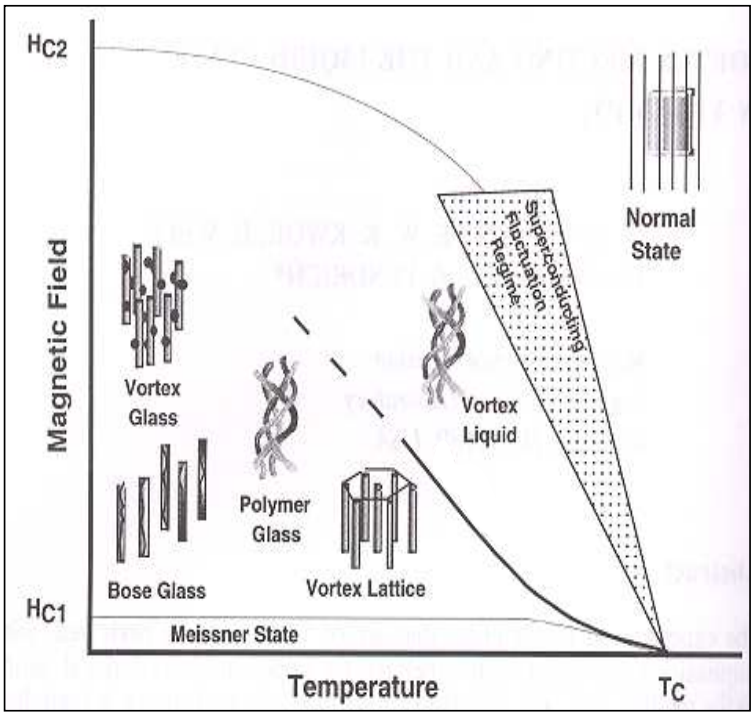

Figure 1.14: Schematic representation of a magnetic phase diagram, showing the different phases that may appear depending on the energy balance.

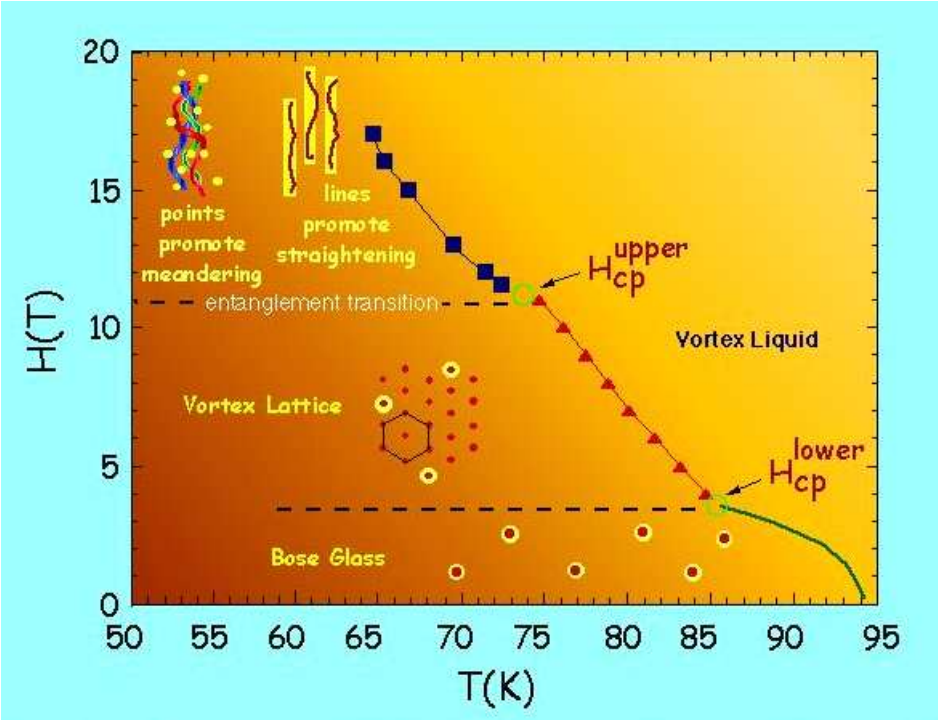

Figure 1.15: Magnetic phase diagram for an untwinned, irradiated single crystal[31]. Shown are the upper and the lower critical point.

present in the sample is enhanced, the vortex solid is transformed into a vortex glass, and the solid-liquid transition becomes broader. The transformation of the first order transition into a second order transition has been widely studied by introducing both, point-like (introduced by electron or proton irradiation) [26] and linear-like defects (introduced through irradiation with ions) [27–30].

Furthermore, for small irradiation doses (and therefore, small densities of defects), a glass and a lattice can coexist in the same sample. In these systems, with moderately low densities of defects, two critical points may develop, arising from the competition between vortex pinning, the elastic energy (i.e. the energy required to distort vortex lines) and the thermal energy [31] (see figure 1.15). These two critical points are defined as the points in the phase diagram where thermal energy, elastic energy and pinning energy coincide [32]. Below the lower critical point and above the upper critical point, the pinning energy is larger than the energy required to distort the lattice, and a glass is formed. At low and high magnetic fields a second order transition is obtained while, for intermediate magnetic fields, the first order transition (signature of the quasi-long range ordered structure) is preserved. The influence of pinning centers in the upper and lower critical point has been studied and it has been shown that columnar defects shift upwards both the lower and the upper critical point while point like defects shift leads to an upwards shift of the lower critical point and a downwards shift

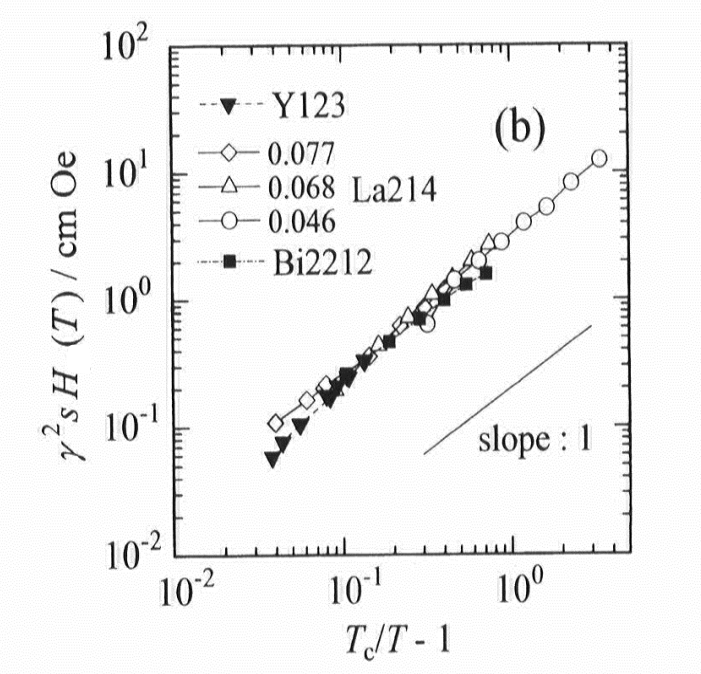

Figure 1.16: Scaling of the melting line when considering the anisotropy of the different samples [33].

of the upper critical point. [31]

An important difference exist between a first order and a second order transition: in the low temperature vortex lattice there is no significant influence of the disorder present in the sample, and, therefore, no action of the underlaying microstructure on the first order transition is to be found. Thus, one should expect an universal behavior of the melting temperature. In agreement with this intrinsic nature of the melting line, it has been reported a scaling of the melting line with the anisotropy of the system (see figure 1.16), where, the liquid region expands to lower temperatures as increasing the anisotropy.

At higher levels of disorder, however, the existence of vortex pinning in the low temperature phase stabilizes this phase against thermal wandering. Therefore, the irreversibility line is shifted upwards, and strongly depends on the particular microstructure of the sample. The study of the position of the solid-liquid transition and its correlation with the microstructure of the samples will be one of the main tools used during this thesis.

At temperatures above the irreversibility line, a pinned vortex liquid may be still found. In a pinned liquid, the vortex viscosity is strongly influenced by the defects but the energy barriers are overcome by thermal fluctuations. Theoretically it is defined when the characteristic time for the vortex to recover spatial homogeneity, τ_{pl}, (limit of an unpinned vortex liquid) is still longer than the characteristic time for the vortices to become unpinned, τ_{pin}. However,

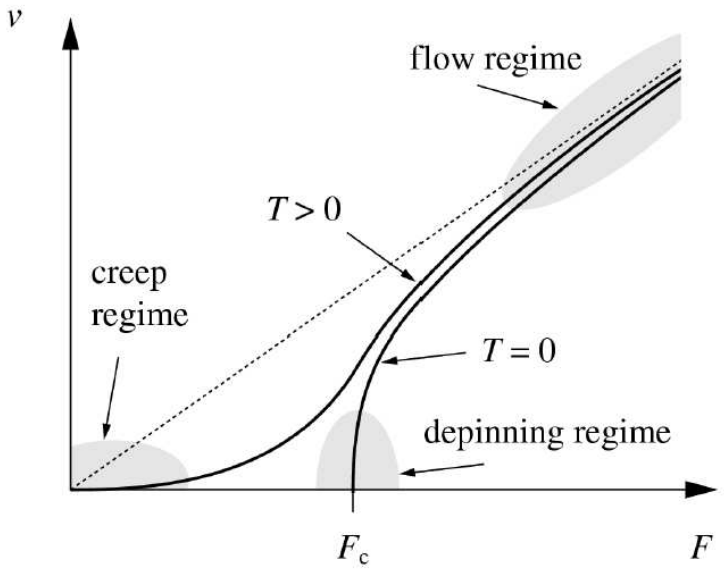

Figure 1.17: Vortex velocity as a function of the driving force. Shown are the different regimes that may be obtained: Flux Creep, Vortex depinning and Flux Flow[35].

the characteristics of the different sorts of pinned liquids and the mechanisms controlling the vortex dynamics are still under debate. Plastic vortex creep in topologically disordered (dislocated) vortex solid phases of type-II superconductors with strong pinning centers has been recently examined theoretically [34].

Together with the strong influence of anisotropy, thermal, pinning energy and vortex-vortex interaction, a strong driving force also may contribute on modifying vortex behavior. This driving force can be produced, for example, by applying an external current circulating through the sample in the presence of an external magnetic field (i.e. a Lorentz force). Depending on its strength and the temperature of the system, several dynamic regimes are obtained:

Depinning: As shown in figure 1.17, at low driving forces (and T=0K), the force acting over the vortex is not able to induce vortex motion. As the driving force, F, is increased beyond a critical value, F_c, the average vortex velocity becomes finite. The value of F_c is determined by the pinning potential that impedes vortex motion.

Flux Flow: At driving forces much larger than the critical force ($F \gg F_c$), i.e. where the barriers are much lower than the applied force, vortices move rapidly and therefore, the pinning potential to which vortices are submitted is averaged, and thus, becomes negligible. For $F \to \infty$, vortices will move in a steady motion with a constant velocity, as they would in a clean sample.

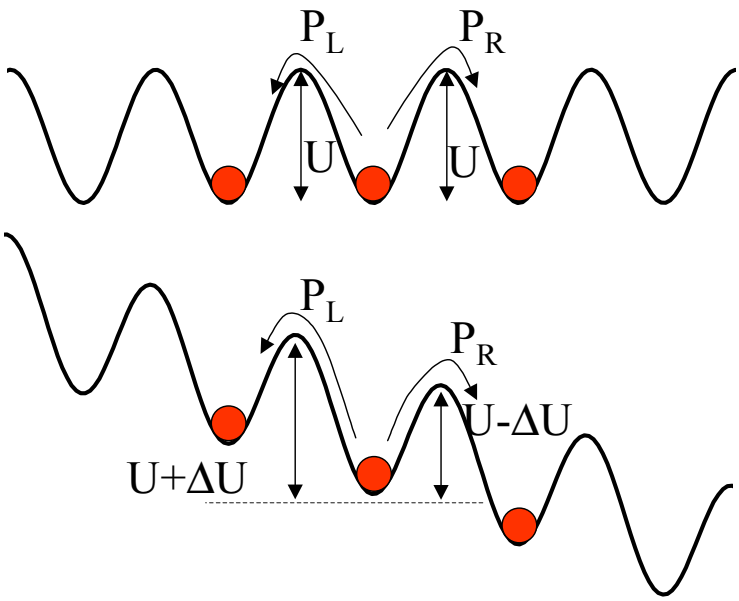

Figure 1.18: Top:profile of the pinning potential in the absence of any applied force. Bottom:profile with an applied current under a magnetic field. Shown are the barriers to be overcame.

Creep: At finite temperatures, however, the presence of a certain thermal energy promotes, even below F_c, vortex motion. In particular, following the Anderson-Kim model [36], vortices are submitted to a pinning barrier given by U (see figure 1.18), with a jump probability $P \propto e^{-U/kT}$. However, the probability is the same for all the directions of the jump and the average velocity vanishes. By applying an electrical current, the barriers are modified and the jump probability is modified, leading to a finite velocity, and therefore, a finite dissipation.

The effective probability of jump parallel to the current is given by:

$$P \propto e^{-U/kT} \cdot \left(e^{\Delta U/kT} - e^{-\Delta U/kT} \right) \propto \langle v \rangle. \tag{1.6}$$

This expression, for applied currents much lower than the depinning one, leads to a thermally assisted flux flow (TAFF) [37]:

$$E \propto v \propto e^{-U/kT} \cdot \frac{J}{J_c} \propto J, \tag{1.7}$$

and therefore to a linear resistivity with an expression analog to 1.5, from where we may extract U; i.e. the height of the barrier impeding vortex motion.

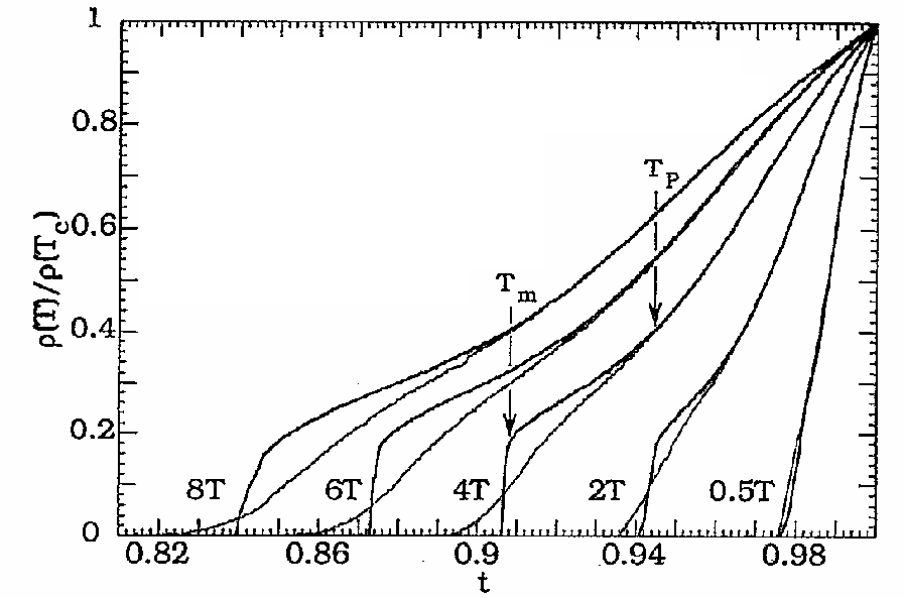

Figure 1.19: Temperature dependence of the resistivity for a clean $YBa_2Cu_3O_{7-\delta}$ single crystal. Also shown for comparison is the temperature dependence of the resistivity for an electron irradiated single crystal (thin lines) [26].

1.3 Phase diagram in $YBa_2Cu_3O_{7-\delta}$ single crystals.

These interactions acting over vortices lead to a wide diversity of behaviors depending on the particular sample and the concrete magnetic field and temperature considered. The characteristics of vortex dynamics have been studied in $YBa_2Cu_3O_{7-\delta}$ single crystals, which, having a low density of defects, represent an excellent scenario to investigate the different phenomena that may appear in HTSC. Although the phenomenologies observed on vortex motion in $YBa_2Cu_3O_{7-\delta}$ single crystals cover a wide region, the goal of this section is, only, to present and summarize the main results observed in single crystals that may be useful for the study of the magnetic phase diagram in melt textured samples.

It was observed that clean $YBa_2Cu_3O_{7-\delta}$ single crystals develop a sharp transition between the solid and the liquid of vortices. Thermodynamic measurements (such as calorimetry [38]) have demonstrated that this is, indeed, a first order transition, from where it follows that the solid has an ordered structure. This first order transition has also been determined by a sharp increase of the resistivity as the temperature is increased above the melting temperature of the sample (T_m)[22] (see figure 1.19). The first order transition, however, is not found in all single crystals since a very low density of defects is able to break the low temperature ordered phase [26].

Together with the existence of this first order transition, the influence of twin boundaries

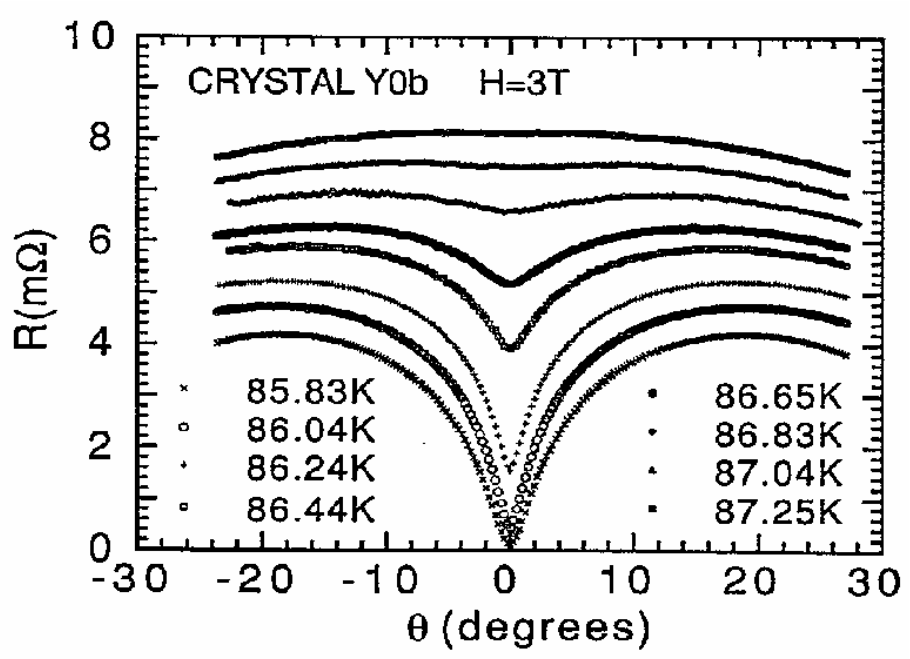

Figure 1.20: Angular dependence of the resistivity for a twinned single crystal at H=3T [39].

in $YBa_2Cu_3O_{7-\delta}$ single crystals has been extensively studied. Two main features were observed in twinned single crystals. The first one showed an increase of vortex pinning for magnetic fields parallels to twin boundaries, reflected in a reduction of the resistivity for H$\|$c in angular dependent measurements (see figure 1.20) [39, 40], which leads to an upwards shift in the solid liquid transition. Later on, the theoretical basis for the influence of columnar defects in this transition (shown to be a Bose-glass transition) was elaborated [17], explaining the upwards shift observed. However, twin boundaries are not pure columnar defects due to their 2-D nature, and consequently, the Bose-glass transition has been mainly studied using columnar tracks introduced by irradiation. In spite of the difference between twin boundaries and columnar tracks, similar qualitative results have been found when the enhancement of vortex pinning is considered.

The second feature observed in single crystals with one family of twin boundaries was an increase of the resistivity for forces acting parallel to twin boundaries. This increase of the resistivity was attributed to vortex channelling through twin boundaries. These different influences of twin boundaries in single crystals will be compared with the results obtained in this work in MTG-$YBa_2Cu_3O_{7-\delta}$ samples where always two twin boundary families are present.

Another issue that has been investigated in single crystals is the existence of vortex correlation across the sample. To do so, flux transformer measurements have been performed on $YBa_2Cu_3O_{7-\delta}$ single crystals. In these measurements, the electrical current at the top of

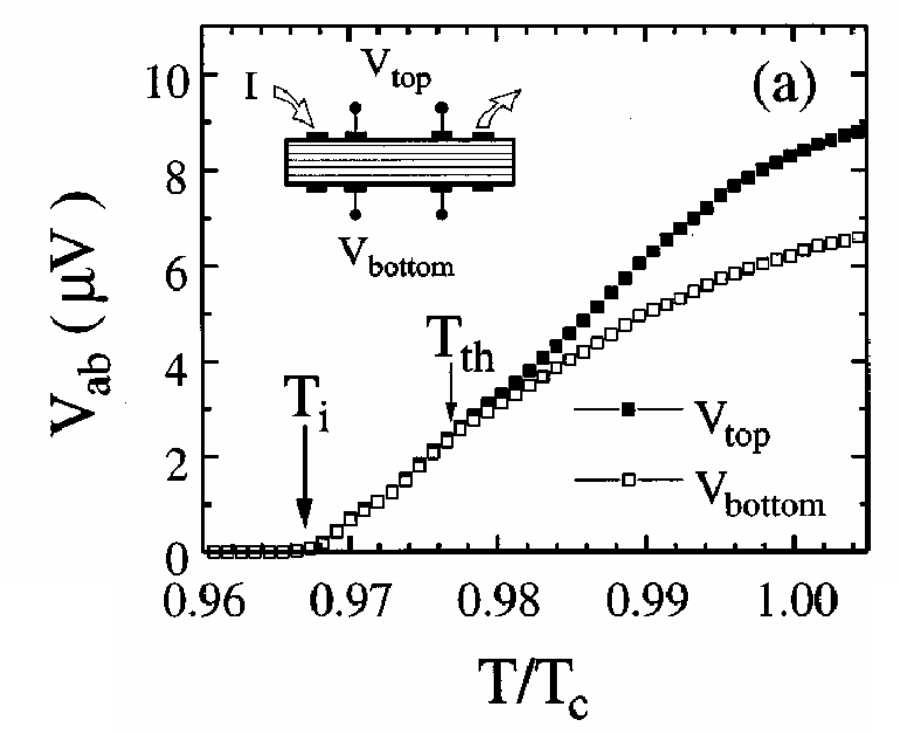

Figure 1.21: Temperature dependence of V^{top} and V^{bot} for a twinned single crystal [41]. Shown in the inset is the scheme of the geometrical configuration used in flux transformer measurements.

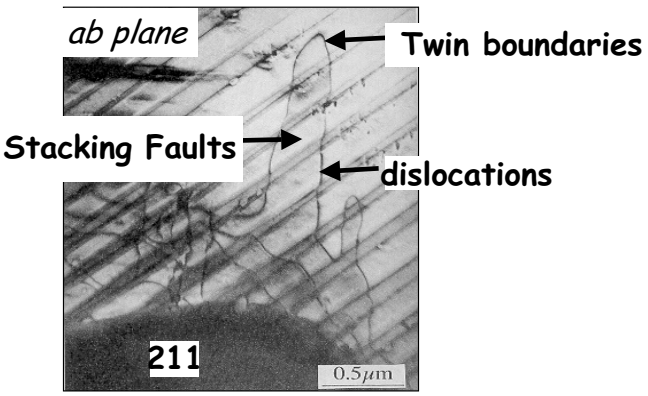

Figure 1.22: Transmission Electron Microscopy (TEM) image of an ab-plane showing the presence of twin boundaries, stacking faults, dislocations and Y_2BaCuO_5 particles.

the sample is larger than that of the bottom, and so does the Lorentz force. Therefore, it will be obtained that the voltage at the top of the sample (V^{top}) is equal to the voltage at the bottom of the sample (V^{bot}) only if full vortex correlation across the sample exist. Although the results obtained are still controversial, it has been shown that full vortex correlation exists in $YBa_2Cu_3O_{7-\delta}$ single crystals below a certain temperature. The existence of full correlation in MTG-$YBa_2Cu_3O_{7-\delta}$ samples will also be studied.

1.4 Melt Textured Grown $YBa_2Cu_3O_{7-\delta}$

1.4.1 Microstructural properties

$YBa_2Cu_3O_{7-\delta}$ single crystals, due to their small dimensions and their reduced critical currents, are not capable to be used in applications where high power is involved. To solve this problem, while still avoiding the presence of grain boundaries, different procedures have been used in order to increase the dimensions [42, 43]. Namely, melt processing techniques which, through a melting process of the $YBa_2Cu_3O_{7-\delta}$ phase and incorporating secondary phases into the $YBa_2Cu_3O_{7-\delta}$ matrix, enable the growth of large single domains (several centimeters). Among these methods of preparation, we have to point out Top Seeding Growth and the Bridgman Method (see page 27), which have been used to grow most of the samples studied in this thesis. The samples thus obtained present a high diversity of defects[44, 45]:

Y_2BaCuO_5 precipitates:

The given preparation methods of large single domains leads to the presence, inside the $YBa_2Cu_3O_{7-\delta}$ matrix, of a high density of small micrometric Y_2BaCuO_5 particles

(up to 40%wt), that are able to have important effects on vortex pinning [46, 47]. In this sense, the presence of CeO_2 (or PtO_2), stopping the growth of these particles and therefore, increasing the surface to volume ratio, is important in order to increase the pinning associated to their interface.

Twin Boundaries:

The similarity between the unit cell parameters *a* and *b* in the crystalline structure of $YBa_2Cu_3O_{7-\delta}$ and the transition existing between the tetragonal and the orthorhombic phase at high temperatures promotes the existence of interfaces between zones having the cell parameters interchanged. These interfaces consist of two families of orthogonal planes (at 45^o from the in-plane crystallographic axis) and containing the c direction (see figure 2.4). Twin boundaries may be able to act as linear pinning centers [48].

Dislocations:

Dislocations are capable to strongly influence vortex pinning in the solid vortex state either acting as point-like or linear-like pinning centers, depending on the direction of the applied magnetic field. Their effects in the liquid vortex state will be widely studied in chapter 5.

Stacking Faults:

$YBa_2Cu_3O_{7-\delta}$ +CuO, under certain conditions is unstable against the formation of $YBa_2Cu_4O_8$, with a structure similar to $YBa_2Cu_3O_{7-\delta}$ but with an extra chain of CuO incorporated into the crystalline structure. Although superconducting, its critical temperature ($T_c \sim$82K) is lower than that of $YBa_2Cu_3O_{7-\delta}$, and therefore, the existence of a local transformation from $YBa_2Cu_3O_{7-\delta}$ to $YBa_2Cu_4O_8$, being an extended planar defect, could have detrimental effects on vortex pinning. The local formation of a unit cell of $YBa_2Cu_4O_8$ is, from a crystallographic point, a stacking fault.

Microcracks:

Melt textured samples, due to their high dimensions and their ceramic character have a high density of microcracks, mainly produced during the oxygen uptake process leading to the tetragonal to orthorhombic transformation. They are parallel to the ab-planes, with a mean separation of the order of several μm. The addition of silver particles modifying the density of ab-microcracks has enabled the study of their influence on the vortex liquid state.

Grain Boundaries:

Two main classes of grain boundaries may exist in these materials: the low angle grain boundaries (with misorientations of $2-3^o$), that do not have strongly detrimental effects on the superconducting properties and the high angle grain boundaries that act as weak link and sharply deteriorate the superconducting properties. The careful preparation of MTG-$YBa_2Cu_3O_{7-\delta}$ samples enables to completely suppress the high angle grain boundaries.

These microstructural characteristics should modify the features of the magnetic phase diagram and vortex dynamics compared to what has been observed in single crystals. Furthermore, these systems provide an excellent opportunity to study the interaction between the influence of different kinds of defects. The importance of this capability is reinforced when it is taken into account the possibility of modifying widely the density of most of these defects. Thus, in this thesis we will employ Melt Textured samples to further investigate the influence of microstructure on the principal points of vortex motion.

1.4.2 Superconducting properties of MTG-$YBa_2Cu_3O_{7-\delta}$

Clearly, the main microstructural characteristic of Melt Textured Grown $YBa_2Cu_3O_{7-\delta}$ samples is the presence of Y_2BaCuO_5 particles embedded in the $YBa_2Cu_3O_{7-\delta}$ matrix. The typical dimensions of these particles are much larger than the coherence length ($\xi \sim 15$Å), thus discarding vortex core pinning at the Y_2BaCuO_5 particles themselves. However, an increase of the critical current density in the vortex solid state was unambiguously found in MTG-$YBa_2Cu_3O_{7-\delta}$ as the density of Y_2BaCuO_5 particles increases [47]. This increase is observed clearer at high temperatures, where the influence of linear, strong pinning centers is expected to be dominant.

Two different mechanisms arose in order to explain this influence. Murakami et al [49], suggested that the clean interface present between the $YBa_2Cu_3O_{7-\delta}$ matrix and the Y_2BaCuO_5 particle could lead to vortex pinning on a length of the order of the size of the particles. Following this argument, critical currents should increase with the area of Y_2BaCuO_5 particles (given by $\frac{V}{\langle d \rangle}$, with V the percentage in volume of Y_2BaCuO_5 and $\langle d \rangle$, the main diameter of these particles) as it has been observed [49]. On the other hand, V.Pan has suggested that the defects present in the interface (such as dislocations and stacking faults) are actually the responsible for this enhancement of pinning [50]. This apparent contradiction among these two alternatives has been recently clarified [51]. The influence of dislocations and stacking faults has also been investigated and its flux pinning influence has been separated from that of Y_2BaCuO_5 particles. In order to study the influence of dislocations and stacking faults in the vortex solid state, different post-treatments have been performed on Melt Textured samples in order to increase their density. The results obtained from magnetic measurements suggest that dislocations (acting as point like pinning centers) leads to an enhancement of pinning (mainly at low temperatures) while an excessive density of stacking faults promotes a reduction of the critical current density [51]. Therefore, the Y_2BaCuO_5 particles leads to an enhancement of the strong pinning contribution while dislocations behave as weak pinning centers [52].

In order to further study the superconducting properties of MTG-$YBa_2Cu_3O_{7-\delta}$ in the vortex solid state and obtain a deeper insight into the influence of the different microstructural characteristics, a new method [52] has been developed to deconvolute the contribution of point like pinning centers (acting as weak pinning centers) from that of linear-like pinning centers (acting as strong pinning centers) in the solid vortex state.

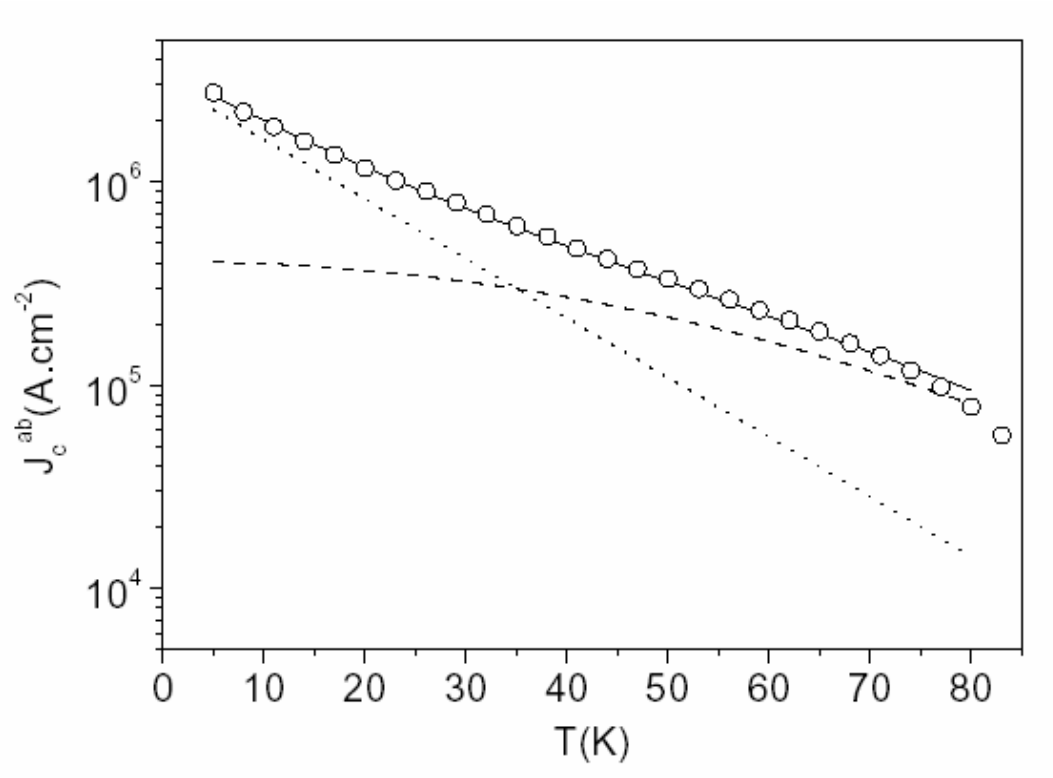

Figure 1.23: Temperature dependence of the critical currents for an MTG-$YBa_2Cu_3O_{7-\delta}$ sample. Shown are the experimental data (○), the contribution from strong pinning centers (dashed line), the contribution from weak pinning centers (dotted line) and the overall contribution (continuous line).

This new methodology takes into account that the different nature of the defects is reflected in the temperature dependence of the inductive critical currents: weak pinning centers lead to an exponential decay of the critical currents[10]: $j(T) = j_c \cdot e^{-\frac{T}{T_0}}$, while for strong pinning centers, the influence of thermal activation decreases, and thus the temperature dependence of the critical currents is softened: $j(T) = j_c \cdot e^{-3\cdot\left(\frac{T}{T^*}\right)^2}$ [17].

Thus, assuming a sample with weak and strong pinning centers, the resulting critical current is, simply, the addition of these contributions:

$$J_c(T) = J_c^{WP} \cdot e^{-\frac{T}{T_0}} + J_c^{SP} \cdot e^{-3\cdot\left(\frac{T}{T^*}\right)^2} \tag{1.8}$$

where, J_c^{WP}, J_c^{SP} are the zero temperature critical currents related to weak pinning and strong pinning centers. T_0 and T^* are related to the energy scale of weak pinning centers and strong pinning centers[16, 17]. Therefore, by adjusting the experimental data for each particular sample, the contribution from weak pinning centers, J_c^{WP} (given by point-like pinning cen-

ters) is distinguished from that of strong pinning centers J_c^{SP} (determined by linear-like pinning centers).[51] An example of the determination of the contribution from weak pinning centers and strong pinning centers is shown in figure 1.23 [51].

This method, and the analysis of the dependence of J_c^{SP} and J_c^{WP} with the densities of the different defects presents in each sample, has enabled to determine the influence of each one of the defects in the vortex solid state.[51] Furthermore, the study of the temperature dependence of the critical currents has been employed in order to check the suitability of the samples prior to their characterization through angular dependent magnetoresistive measurements.

In the vortex liquid state, magnetoresistive measurements in MTG-$YBa_2Cu_3O_{7-\delta}$ materials clearly differ from those of clean single crystals since the first order transition between the solid and the liquid state disappears, thus reflecting that the disorder present in textured samples breaks the long range order characteristic of systems where the vortex-vortex interaction is dominant.

In spite of the existence of this strong difference, there are, on the other hand, important similarities between the properties of both types of samples: firstly, the anisotropic behavior observed in single crystals between a c-axis and a ab-plane magnetic field is reproduced in Melt Textured Grown $YBa_2Cu_3O_{7-\delta}$ samples, in spite of the low angle grain boundaries present in these samples. Secondly, the dip in the resistivity observed in angular dependent measurements for magnetic fields parallels to columnar defects (either twin boundaries or columnar tracks) is also present in melt textured samples with a high density of twin boundaries [48]. These similarities and differences between $YBa_2Cu_3O_{7-\delta}$ single crystals and MTG-$YBa_2Cu_3O_{7-\delta}$ samples will be further explored in chapter 3.

Flux transformer measurements have also been performed on Melt Textured Samples, thus enabling further comparison between clean single crystals and textured samples. Similarly to single crystals, it was previously shown [53] that a certain correlation exists across the sample for H||c up to a given temperature. Initial works showed that this correlation, however, was not complete, and thus it was suggested that Y_2BaCuO_5 particles could generate a loss of full vortex correlation in the system. However it has been recently shown that full correlation may also exist in melt textured samples[54].

The goal of this thesis is to investigate the influence of the microstructure on the superconducting properties in the vortex liquid state of Melt Textured Grown $YBa_2Cu_3O_{7-\delta}$ samples. In particular, the influence of the $YBa_2Cu_3O_{7-\delta}/Y_2BaCuO_5$ interface, dislocations (as linear-like and point-like pinning centers), microcracks, stacking faults and twin boundaries has been investigated. The results obtained for this wide diversity of defects will be used to further investigate the vortex liquid phase diagram and explore the properties of vortex motion.